

This work was written as part of one of the author's official duties as an Employee of the United States Government and is therefore a work of the United States Government. In accordance with 17 U.S.C. 105, no copyright protection is available for such works under U.S. Law.

Public Domain Mark 1.0

<https://creativecommons.org/publicdomain/mark/1.0/>

Access to this work was provided by the University of Maryland, Baltimore County (UMBC) ScholarWorks@UMBC digital repository on the Maryland Shared Open Access (MD-SOAR) platform.

Please provide feedback

Please support the ScholarWorks@UMBC repository by emailing scholarworks-group@umbc.edu and telling us what having access to this work means to you and why it's important to you. Thank you.

Unsupervised interference rejection approach to target detection and classification for hyperspectral imagery

Chein-I Chang, MEMBER SPIE

Tzu-Lung Sun

University of Maryland, Baltimore County
Department of Computer Science
and Electrical Engineering
Remote Sensing Signal and Image
Processing Laboratory
1000 Hilltop Circle
Baltimore, Maryland 21250

Mark L. G. Althouse, MEMBER SPIE

U.S. Army
Edgewood Research Development and
Engineering Center
SCBRD-RTE
Aberdeen Proving Ground, Maryland
21010-5423

Abstract. A widely used approach to hyperspectral image classification is to model a mixed-pixel vector as a linear superposition of substances resident in a pixel with additive Gaussian noise. Using this linear mixture model many image processing techniques can be applied, such as linear unmixing or orthogonal subspace projection. However, a third source not considered in this model, called interference (clutter or structured noise), may sometimes give rise to more serious signal deterioration than the additive noise. We address this issue by introducing the interference into the linear mixture model. Including interference in the model enables us to treat the interference as another undesired source, like a passive jammer, so that it can be eliminated prior to detection and classification. This is particularly useful for hyperspectral images, which tend to have a high SNR but a low signal-to-interference ratio with the interference difficult to identify. To find and reject interference, we propose an unsupervised vector quantization-based interference rejection (UIR) approach in conjunction with either an orthogonal subspace projection (OSP) or an oblique subspace projection (OBSP) to simultaneously project a pixel into signature space as well as to null out interference. Since there is no prior knowledge about the interference, the UIR is implemented in an unsupervised manner to generate the desired interference clusters so that they can be annihilated by the OSP or OBSP. The proposed approach is shown by evaluation with Hyperspectral Digital Imagery Collection Experiment (HYDICE) data to exhibit considerable improvement in comparison to linear unmixing or the OSP where interference is not considered. © 1998 Society of Photo-Optical Instrumentation Engineers. [S0091-3286(98)00103-2]

Subject terms: classification; detection; hyperspectral image; interference rejection; oblique subspace projection; orthogonal subspace projection; vector quantization.

Paper ART-104 received May 23, 1997; revised manuscript received Aug. 10, 1997; accepted for publication Aug. 10, 1997.

1 Introduction

Recently, remote sensing has advanced to the point where a new generation of sensors, called imaging spectrometers, has been developed to fine-tune spectral resolution so that materials with very similar spectra, which can not be resolved by multispectral imagers such as the multispectral scanner (MSS) and Thematic Mapper (TM), can be discriminated and quantified. Examples of such sensors include the airborne visible/infrared imaging spectrometer (AVIRIS) developed by the National Aeronautics and Space Administration (NASA) Jet Propulsion Laboratory and the Hyperspectral Digital Imagery Collection Experiment (HYDICE) sensor developed by Naval Research Laboratory. The concept of developing such high-resolution spectral sensors, typically with 20 to 40-nm spectral resolution, is to take advantage of contiguous, inherently registered spectral bands to capture diagnostic narrow-band spectral features present in the pixels so that their corresponding materials can be uniquely identified.¹

Spectral unmixing has been widely used in the remote sensing community to quantify and identify the materials resident in multispectral and hyperspectral images.² A recent approach, orthogonal subspace projection³ (OSP), was also proposed for hyperspectral image classification and has shown promise in HYDICE data exploitation. The OSP has been further extended and generalized in various contexts.⁴⁻⁶ All these approaches are based on the fact that an image pixel is linearly mixed by the materials within the pixel and corrupted by an additive Gaussian noise. By taking advantage of this linear mixture model, many existing image processing techniques that cannot be directly applied to multispectral/hyperspectral image analysis can now be adapted and modified to fit different applications in remote sensing. However, the assumed linear mixture model involves only signal and noise sources with interference generally discarded or included in noise/signals. Since hyperspectral sensors use as many as 200 contiguous bands to capture the subtle discrepancies between spectral signatures, it may also extract many unwanted signatures such as clutter and background. These unwanted signatures can be

viewed as interferers and must be eliminated before data processing. Consequently, this presents another mixing problem and further complicates the situation. It has been noted in HYDICE data that hyperspectral images tend to have a high SNR but a low signal-to-interference ratio. As a result, including interference as another distinct source in the linear mixture model can be beneficial. In this paper, we address this issue by modeling interference as a separate third source in addition to target signatures and noise. The advantage of introducing interference into the model is that it can separate the unwanted interference from signatures of interest so that they can be removed early. To do so, an unsupervised vector quantization (VQ)-based interference rejection (UIR) approach is proposed in conjunction with either an OSP (Ref. 3) or an oblique subspace projection⁶ (OBSP). The UIR is a clustering and interference generation process which produces a desired set of interference signatures that can be annihilated or suppressed prior to detection and classification so as to achieve signal enhancement. Due to the fact that no prior knowledge about the interference is available, the UIR employs unsupervised VQ (Ref. 5) to generate interference clusters, each of which represents a certain type of interference. These clusters are then annihilated by either the OSP or the OBSP. The number of interference clusters required for the UIR is determined by rank curves that are generated based on two different criteria, orthogonal projection divergence for OSP and eigenvalues for OBSP. It is shown through HYDICE data that the UIR approach is a significant improvement over the OSP or OBSP approaches with no interference considered in the linear mixture model.

This paper is organized as follows. Section 2 formulates the hyperspectral image classification as a linear mixing problem and Sec. 3 briefly reviews subspace projection approaches including OSP and OBSP. Section 4 describes a VQ-based clustering process. Section 5 presents the complete implementation of a UIR approach, where the OSP and OBSP classifiers are used for target classification. Section 6 conducts experiments using HYDICE data to demonstrate the advantage of the UIR. Finally, a conclusion is given in Sec. 7.

2 Linear Mixture Model

Linear spectral mixing is a widely used approach in remotely sensed imagery to determine and quantify multicomponents. Since every pixel is comprised of discrete spectral bands, it can be represented by a column vector whose components are pixels in these individual spectral bands. More precisely, suppose that l is the number of spectral bands. Let \mathbf{r}_i be an $l \times 1$ column vector and denote the i 'th pixel in a hyperspectral image where the bold face is used for vectors. So, each pixel is represented by a pixel vector with dimensionality l and a hyperspectral image can be viewed as an image cube. Assume that \mathbf{M} is an $l \times p$ signature matrix denoted by $(\mathbf{m}_1, \mathbf{m}_2, \dots, \mathbf{m}_p)$, where \mathbf{m}_j is an $l \times 1$ column vector, which represents the j 'th signature (substance) resident in the pixel \mathbf{r}_i and p is the number of these signatures. These signatures are generally target signatures of interest to be classified. Let α_j

$= (\alpha_{i1} \alpha_{i2} \dots \alpha_{ip})^T$ be a $p \times 1$ abundance column vector associated with \mathbf{r}_i , where α_{ij} denotes the abundance concentration of the j 'th signature in the pixel \mathbf{r}_i .

A widely used linear mixture model in linear unmixing assumes that the substances present in a pixel vector are linearly superpositioned. Statistically, it can be represented by a linear regression model as follows:

$$\mathbf{r}_i = \mathbf{M}\alpha_i + \mathbf{n}_i, \quad (1)$$

where \mathbf{n}_i is an $l \times 1$ column vector representing additive white Gaussian noise with zero mean and variance $\sigma^2 \mathbf{I}$ and \mathbf{I} is the $l \times l$ identity matrix.

3 Subspace Projection Approaches to Hyperspectral Image Classification

A classical approach to solving Eq. (1) is to find a matrix inverting Eq. (1) so that the multicomponents mixed in the pixel vector \mathbf{r}_i can be identified separately. This procedure is generally referred to as linear unmixing. Since the number of bands l is usually much greater than that of signatures p in hyperspectral images, Eq. (1) is overdetermined and not full rank. Simply inverting the signature matrix will result in singularities. In that case, singular value decomposition (SVD) could be used to proceed.⁷ In a recent study,³ an OSP approach was shown to be a promising alternative and has proved to be effective in AVIRIS and HYDICE data exploitation. In this section, we first review the OSP technique and then another subspace projection,⁶ called OBSP.

3.1 OSP

First, we rewrite the model of Eq. (1) as

$$\mathbf{r} = \mathbf{d}\alpha_p + \mathbf{U}\gamma + \mathbf{n}, \quad (2)$$

where the subscript i is suppressed, $\mathbf{U} = (\mathbf{m}_1, \mathbf{m}_2, \dots, \mathbf{m}_{p-1})$ is the undesired spectral signature matrix comprising a set of the first $p-1$ signatures, and $\mathbf{d} = \mathbf{m}_p$ is a desired signature. Here, we assume without loss of generality that the last signature is the desired signature \mathbf{d} to be classified. Note that Eq. (2) can be extended straightforwardly to more than one desired signature. The reason of separating \mathbf{U} from \mathbf{M} is to enable us to design an orthogonal subspace projector to annihilate \mathbf{U} from an observed pixel prior to classification. One such projector is an undesired signature annihilator, denoted by \mathbf{P}_U^\perp , given by

$$\mathbf{P}_U^\perp = \mathbf{I} - \mathbf{U}\mathbf{U}^\#, \quad (3)$$

where $\mathbf{U}^\# = (\mathbf{U}^T \mathbf{U})^{-1} \mathbf{U}^T$ is the pseudoinverse of \mathbf{U} and the notation \perp_U in \mathbf{P}_U^\perp indicates that the projector \mathbf{P}_U^\perp maps the observed pixel \mathbf{r} into the space $\langle \mathbf{U} \rangle^\perp$, the orthogonal complement of $\langle \mathbf{U} \rangle$ (Ref. 3).

Now, applying \mathbf{P}_U^\perp to the model of Eq. (2) results in a new spectral signature model

$$\mathbf{P}_U^\perp \mathbf{r} = \mathbf{P}_U^\perp \mathbf{d}\alpha_p + \mathbf{P}_U^\perp \mathbf{n}, \quad (4)$$

where the undesired signatures in \mathbf{U} have been eliminated and the original noise has been suppressed to $\mathbf{P}_U^\perp \mathbf{n}$.

Equation (4) represents a standard signal detection problem. If the optimal criterion for the signal detection problem specified by Eq. (4) is chosen to maximize the SNR given by

$$\text{SNR} = \frac{(\mathbf{x}^T \mathbf{P}_U^\perp \mathbf{d}) \alpha_p^2 (\mathbf{d}^T \mathbf{P}_U^\perp \mathbf{x})}{\mathbf{x}^T \mathbf{P}_U^\perp E(\mathbf{n}\mathbf{n}^T) \mathbf{P}_U^\perp \mathbf{x}}, \quad (5)$$

over \mathbf{x} , then the maximum SNR of Eq. (5) can be obtained by a matched filter, denoted by \mathbf{M}_d using $\mathbf{x} = \kappa \mathbf{d}$ with a constant κ and the matched signal \mathbf{d} .

Based on the approach outlined by Eqs. (4) and (5), a mixed pixel classification can be carried out by a two-stage process, an undesired signature annihilator \mathbf{P}_U^\perp followed by a matched filter, \mathbf{M}_d . More precisely, if we want to classify a desired signature, say \mathbf{d} in a mixed pixel based on the model of Eq. (1), we first apply \mathbf{P}_U^\perp to the model of Eq. (2) to eliminate \mathbf{U} , then we use the matched filter \mathbf{M}_d to extract \mathbf{d} from the signal detection model of Eq. (4). The operator coupling \mathbf{P}_U^\perp with \mathbf{M}_d is called an orthogonal subspace classifier, \mathbf{P}_{OSP} derived in Ref. 3 and denoted by

$$\mathbf{P}_{\text{OSP}} = \mathbf{M}_d \mathbf{P}_U^\perp = \mathbf{d}^T \mathbf{P}_U^\perp. \quad (6)$$

3.2 Linear Spectral Signal-Interference Mixture Model

According to experiments using HYDICE data, it was found that hyperspectral images generally had a high SNR but a low signal-to-interference ratio. This means that the interference sometimes presents more serious contribution than noise to performance degradation. However, from the model of Eq. (1), the interference is either assumed to be discarded or included in noise or signals. In the latter case, if the interference is included in the noise, it cannot be additive and independent as assumed in the model Eq. (1). If the interference is included in signals, it must be specified. On the other hand, if it is ignored, the interference serves as a passive jammer. Therefore, it must be considered separately and further be removed prior to detection and classification. In either case, the model of Eq. (1) may not be adequate for hyperspectral images. To take care of this problem, we introduce the interference as a third separate source in the model of Eq. (1). In this formulation, the signatures in \mathbf{M} are only those required to be classified and the interference will be treated separately as unknown but unwanted signatures in the image. In addition, the noise is additive Gaussian noise independent of signature and interference. Such a model is called a linear spectral signature-interference mixture model in this paper and can be described as follows.

Let $\mathbf{S} = (\mathbf{s}_1 \mathbf{s}_2 \dots \mathbf{s}_q)^T$ be the interference matrix where \mathbf{s}_k is the k 'th interference signature and $\boldsymbol{\phi}_i = (\phi_1 \phi_2 \dots \phi_q)^T$ is the corresponding abundance vector of the interference signatures in \mathbf{S} . A linear spectral signature-interference mixture model for \mathbf{r}_i modified from the model of Eq. (1) can be derived by

$$\mathbf{r}_i = \mathbf{M} \boldsymbol{\alpha}_i + \mathbf{S} \boldsymbol{\phi}_i + \mathbf{n}_i. \quad (7)$$

3.3 OBSP

The OBSP was developed based on a concept of enhancing signals while nulling interference. Several applications of the OBSP were discussed and studied in array processing and communications.⁸ A new application of the OBSP to hyperspectral image classification was recently reported,⁶ which can be viewed as an *a posteriori* OSP method. The idea is to take advantage of the ability of the OBSP in signal enhancement, noise suppression, and interference annihilation. By relying on Eq. (7) we can develop a method that uses the OBSP as an interference rejecter to eliminate interference signatures in \mathbf{S} before target detection.

Let $\langle \mathbf{M} \rangle$ and $\langle \mathbf{S} \rangle$ be the spaces linearly spanned by \mathbf{M} and \mathbf{S} , respectively. The OBSP is applied to hyperspectral image pixels by specifying $\langle \mathbf{M} \rangle$ as its range space and $\langle \mathbf{S} \rangle$ as its null space. As a result \mathbf{S} will be eliminated via the OBSP while the pixel will be projected into the signature space \mathbf{M} . From Ref. 7, a desired OBSP-based interference rejecter can be derived by

$$E_{\mathbf{MS}} = \mathbf{M}(\mathbf{M}^T \mathbf{P}_S^\perp \mathbf{M})^{-1} \mathbf{M}^T \mathbf{P}_S^\perp, \quad (8)$$

where the first and second subscripts in $E_{\mathbf{MS}}$ denote the range space \mathbf{M} and the null space \mathbf{S} respectively and $E_{\mathbf{MS}} \mathbf{M} = \mathbf{M}$ and $E_{\mathbf{MS}} \mathbf{S} = 0$. The \mathbf{P}_S^\perp in Eq. (8) is referred to as the interference annihilator and is defined in the same fashion as Eq. (3) by

$$\mathbf{P}_S^\perp = \mathbf{I} - \mathbf{S} \mathbf{S}^\# = \mathbf{I} - \mathbf{P}_S, \quad (9)$$

and

$$\mathbf{P}_S = \mathbf{S} \mathbf{S}^\#, \quad (10)$$

where $\mathbf{S}^\# = (\mathbf{S}^T \mathbf{S})^{-1} \mathbf{S}^T$ is the pseudoinverse of \mathbf{S} .

4 VQ

In the model of Eq. (7), the interference matrix \mathbf{S} is assumed to be known. Unfortunately, a description of \mathbf{S} is generally not available in practice and must be obtained from the data. In this section, an unsupervised VQ-based clustering process⁵ is proposed to automatically generate a desired interference matrix \mathbf{S} for the model of Eq. (7). The only assumption made in this approach is that the number of interference signatures must be given *a priori*. However, this number can be determined by rank curves as demonstrated in experiments. The VQ procedure described next is based on the well-known Linde-Buzo-Gray (LBG) algorithm⁹ and the criterion for optimality to be used is the mean squared error (MSE).

4.1 VQ

Assuming that q is the number of codewords to be generated for a codebook, the VQ algorithm is as follows

1. Initialization: $\text{Code}^1 = \{\mathbf{x}_j^1\}_{j=1}^q$, where $\{\mathbf{x}_j^1\}_{j=1}^q$ is a set of q initial clusters generated by an algorithm.¹⁰
2. Iterative procedure for reclustering at step $i > 1$ to generate the i 'th code book $\text{Code}^i = \{\mathbf{x}_j^i\}_{j=1}^q$:

$$\mathbf{x}_j^i = E(\mathbf{X} | \mathbf{X} \in R_j^{i-1}) \quad (11)$$

where R_j^{i-1} is the j 'th cluster produced by the codebook at step $i-1$, $\text{Code}^{i-1} = \{\mathbf{x}_j^{i-1}\}_{j=1}^q$.

3. Stopping rule: The reclustering will be terminated when no more data vectors are shuffled from one cluster to another. More specifically, as the algorithm iterates, the MSE between data vectors and their nearest cluster centers will be reduced until there is no change in the codebook. As a result, either the MSEs in two consecutive iterations remain unchanged or their difference is below a prescribed threshold. In this case, no data vector will be shuffled.

5 UIR Approaches

After a desired set of q interference clusters is generated by the VQ algorithm, two approaches can be used to annihilate these q interference signatures. One is the OSP-based unsupervised interference rejection (OSPUIR) approach, which treats the interference signatures as part of undesired signatures. In this case, the \mathbf{U} described in Eq. (2) is augmented by including the interference matrix \mathbf{S} in \mathbf{U} . A second approach, called oblique subspace-based unsupervised interference rejection (OBSPUIR), uses the OBSP $E_{\mathbf{MS}}$ in Eq. (8) to annihilate these q interference signatures. After interference elimination, the signature matrix \mathbf{M} is further decomposed into a target signature, denoted by \mathbf{d} and undesired signature vectors in \mathbf{U} as described in the model of Eq. (2). Then a second OBSP operator defined by $E_{\mathbf{dU}} = \mathbf{d}(\mathbf{d}^T \mathbf{P}_{\mathbf{U}}^\perp \mathbf{d})^{-1} \mathbf{d}^T \mathbf{P}_{\mathbf{U}}^\perp$ via Eq. (8) is applied again to extract the target signature. Thus, in the OBSP approach, the first OBSP, $E_{\mathbf{MS}}$, is served as an interference annihilator and the second OBSP, $E_{\mathbf{dU}}$, is used as a target classifier. The major difference between OSPUIR and OBSPUIR is that the former is an *a priori* approach, which assumes the abundance of all signatures in the model of Eq. (7) is known *a priori*, while the latter is considered to be an *a posteriori* approach, where the abundance of signatures in \mathbf{M} and \mathbf{S} must be estimated from the data. As shown in Ref. 6, the OSP and OBSP classifiers detected different fractions of abundance for target signatures despite the fact that they both produced the same classification feature vector. However, for the OSPUIR to generate desired interference signatures for annihilation, we apply an operator $\mathbf{P}_{\mathbf{M}}^\perp = \mathbf{I} - \mathbf{M}\mathbf{M}^\dagger$, which is defined in a similar fashion to Eq. (3) to project all image pixels into the orthogonal complement space of the signature space generated by \mathbf{M} . As a result⁴ of $\mathbf{P}_{\mathbf{M}}^\perp$, the *a priori* OSPUIR becomes a *a posteriori* classifier as is the OBSPUIR classifier and both the OSP-based and OBSP-based classifiers will produce nearly the same results. This fact will be demonstrated by HYDICE data in Sec. 6. Note that the interference considered in this paper is not limited to background interference, which usually can be determined by inspection, e.g., grass, trees, but also includes interferers that can be difficult to identify from the data.

In contrast to the OSPUIR, the OBSPUIR is carried out in a two stage process. The first stage is to design an interference annihilator and then develop an OBSP-based classifier in the second stage to eliminate the undesired signa-

tures. The OSPUIR and OBSPUIR are summarized as follows.

5.1 OSPUIR

1. Initial condition: Select a set of target signatures \mathbf{M} .
2. Find the orthogonal complement space of \mathbf{M} . Apply $\mathbf{P}_{\mathbf{M}}^\perp = \mathbf{I} - \mathbf{M}\mathbf{M}^\dagger = \mathbf{I} - \mathbf{M}(\mathbf{M}^T \mathbf{M})^{-1} \mathbf{M}^T$ via Eq. (3) to all image pixel vectors \mathbf{r} .
3. Find interference signatures using VQ. Use VQ to generate q clusters with the j 'th center or centroid denoted by \mathbf{s}_j . These centers constitute a set of q interference signatures $\{\mathbf{s}_1, \mathbf{s}_2, \mathbf{s}_3, \dots, \mathbf{s}_q\}$. Let $\mathbf{S} = (\mathbf{s}_1 \mathbf{s}_2 \dots \mathbf{s}_q)$.
4. Apply the OSP classifier given by Eq. (6) with $\mathbf{U} = (\mathbf{m}_1 \mathbf{m}_2 \dots \mathbf{m}_{p-1} \mathbf{S})$ to extract \mathbf{d} .

The complete execution of OSPUIR can be expressed in terms of the following mathematical operations

$$\mathbf{P}_{\text{OSPUIR}} = \mathbf{P}_{\text{OSP}}(\mathbf{VQ}) \mathbf{P}_{\mathbf{M}}^\perp = \mathbf{d}^T \mathbf{P}_{\mathbf{U}}^\perp (\mathbf{VQ}) \mathbf{P}_{\mathbf{M}}^\perp, \quad (12)$$

where $\mathbf{M} = (\mathbf{m}_1 \mathbf{m}_2 \dots \mathbf{m}_{p-1} \mathbf{d})$ and $\mathbf{U} = (\mathbf{m}_1 \mathbf{m}_2 \dots \mathbf{m}_{p-1} \mathbf{S})$.

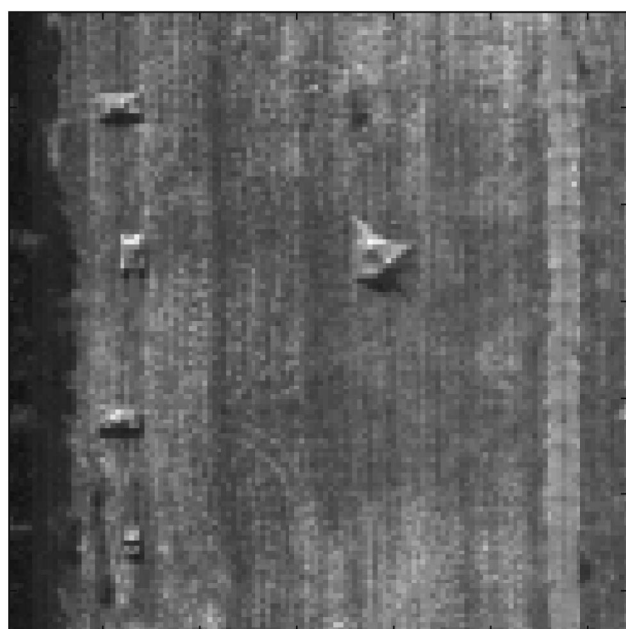
5.2 OBSPUIR

1. Initial condition: Select a set of target signatures \mathbf{M} .
2. Find the orthogonal complement space of \mathbf{M} . Apply $\mathbf{P}_{\mathbf{M}}^\perp$ via Eq. (9) to all image pixel vectors \mathbf{r} .
3. Find interference classes using VQ. Use VQ to generate q clusters with the j 'th center or centroid denoted by \mathbf{s}_j . These centers constitute a set of q interference signatures $\{\mathbf{s}_1, \mathbf{s}_2, \mathbf{s}_3, \dots, \mathbf{s}_q\}$. Let $\mathbf{S} = (\mathbf{s}_1 \mathbf{s}_2 \dots \mathbf{s}_q)$.
4. Eliminate the interference classes using the interference rejecter $E_{\mathbf{MS}}$. Now apply an OBSP operator $E_{\mathbf{MS}}$ given by Eq. (8) with $\mathbf{M} = (\mathbf{m}_1 \mathbf{m}_2 \dots \mathbf{m}_{p-1} \mathbf{d})$.
5. Null the undesired signatures in $\mathbf{U} = (\mathbf{m}_1 \mathbf{m}_2 \dots \mathbf{m}_{p-1})$ and extract the target using the OBSP classifier $E_{\mathbf{dU}}$.

The OBSPUIR is carried out by two oblique subspace projections in conjunction with a VQ-based clustering process described as follows.

$$\mathbf{P}_{\text{OBSPUIR}} = E_{\mathbf{dU}} E_{\mathbf{MS}} (\mathbf{VQ}) \mathbf{P}_{\mathbf{M}}^\perp. \quad (13)$$

Note that the OBSP used in step 5 of the OBSPUIR can be replaced by the OSP given by Eq. (6) to achieve the nearly the same classification results. This is because it was shown^{4,6} that when the OBSP and the OSP are applied to the model of Eq. (2), they both produce the same classification feature vector $\mathbf{d}^T \mathbf{P}_{\mathbf{U}}^\perp$ with a constant difference in their magnitudes given by $(\mathbf{d}^T \mathbf{P}_{\mathbf{U}}^\perp \mathbf{d})^{-1}$. This constant alters only the fraction of abundance detected in the classified pixels but does not affect the classification performance.



A HYDICE image scene

Fig. 1 HYDICE image scene.

6 Experiments Using HYDICE Data

In this section, we describe experiments using hyperspectral images that illustrate the advantages of using the linear signature-interference spectral mixture model [Eq. (7)].

The HYDICE data used in the experiments are an image scene taken in Maryland in August 1995 using 210 bands of 10-nm spectral resolution with the coverage 0.4 to 2.5 μm and the average ground sampling distance (GSD) ranging from 1 to 4 m. However, for illustrative purposes we selected an image scene collected by a low-altitude flight and the GSD is approximately 0.78 m. A 128×128 subimage was cropped from this image and is shown in Fig. 1. This figure shows a single-band image scene (band 30) with tree lines along the left one eighth and a grass field in the right seven eighths. This grass field also contains a road running along the right edge of the image. Four vehicles along the tree line are vertically aligned. The top three are treaded vehicles and the bottom one is a wheeled vehicle. The size of treaded vehicles is approximately 4×8 m and the size of the wheeled vehicle is about 3×6 m. There is one object located near the center of the scene. The experiment is designed to demonstrate a situation when only partial knowledge of the signatures is available.

Suppose that three signatures are of interest and they will serve as the targets to be classified: the three treaded vehicles, the wheeled vehicle, and the object. There are some partial knowledge about the background, which can help to determine background interference signatures. Let the trees, the grass, and the road be such background signatures. Let [the first treaded vehicle signature, the wheeled vehicle signature, the object signature] be the target matrix, denoted by \mathbf{T} and [tree signature, grass signature, road signature] be the background matrix denoted by \mathbf{B} . The first experiment was conducted to see how \mathbf{B} affects the classification performance. The images in the first, second and

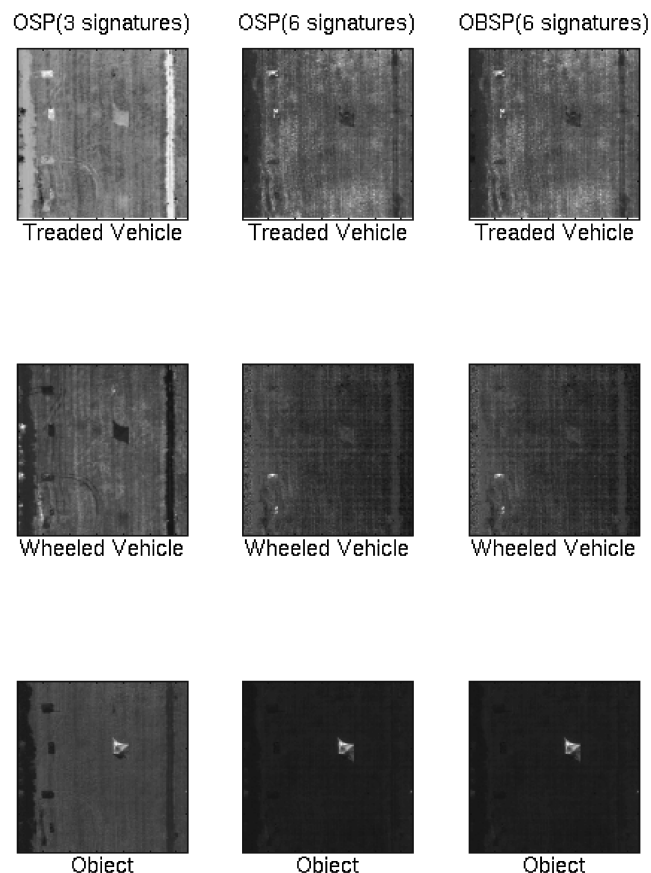


Fig. 2 First column is the results produced by the OSP with $\mathbf{M}=\mathbf{T}$, the second column is the results produced by the OSP with $\mathbf{M}=\mathbf{TUB}$, and the third column is the results produced by the OBSP with $\mathbf{M}=\mathbf{TUB}$.

third columns of Fig. 2 were obtained by the OSP with $\mathbf{M}=\mathbf{T}$, the OSP with $\mathbf{M}=\mathbf{TUB}$ and the OBSP using $E_{\mathbf{MS}}$ with $\mathbf{M}=\mathbf{TUB}$, respectively, where one of the target signatures was designated as the desired signature \mathbf{d} and \mathbf{U} consisted of the other two undesired target signatures. As can be seen, the classification was greatly improved by including the background matrix \mathbf{B} . In addition, the figure also shows that both OSP and OBSP produced nearly the same results. It is interesting to note that in Fig. 2, the third treaded vehicle was missed when the treaded vehicles were classified. Instead, it was picked up in the wheeled vehicle classification. This occurrence is not surprising because the spectrum of the third treaded vehicle is very similar to that of the wheeled vehicles as shown in Fig. 3. As a result, classifying one will detect the other.

In the HYDICE image scene, we could obtain by inspection some partial interference from the data such as background signatures. However, there are many other types of unknown interference signatures, which deteriorate the classification performance. To identify possible interference signatures including unobservable ones, an unsupervised VQ-based clustering process was used to generate a class of clusters that is used to form the interference matrix \mathbf{S} . The images in the first column of Fig. 4 were obtained by the OSPUIR with 10 interference signatures generated

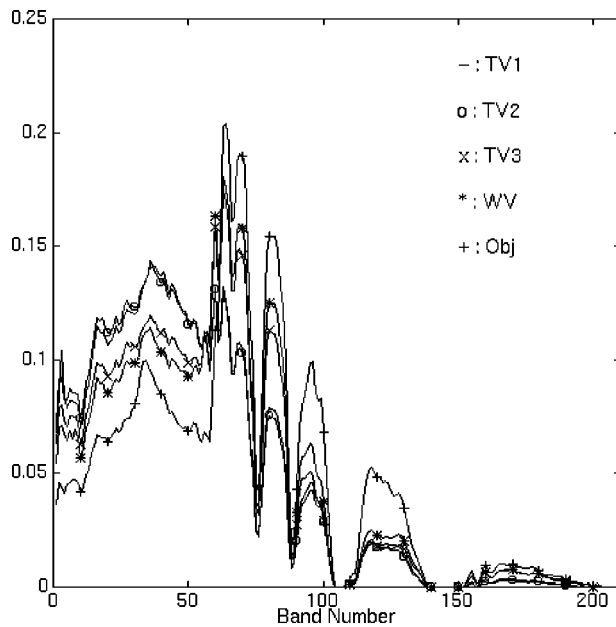


Fig. 3 Spectra of the three treaded vehicles, the wheeled vehicles, and the object.

by VQ to form the interference matrix \mathbf{S} as part of the signature matrix \mathbf{M} (i.e., $\mathbf{M}=\mathbf{TUBS}$). The second column of Fig. 4 shows the images obtained by OSPUIR with $\mathbf{M}=\mathbf{TUB}$ as the signature matrix and with \mathbf{S} as the interference matrix. Comparing Fig. 4 to Fig. 2, the image classification in Fig. 4 is significantly improved because the images in Fig. 4 have eliminated interference signatures, which were not considered in Fig. 2.

Since there is no knowledge about how many interference signatures needed to be generated by VQ, the quantity $\eta=\mathbf{d}^T\mathbf{P}_{\mathbf{U}}\mathbf{d}$, called orthogonal projection correlation index is used as a criterion for OSPUIR to determine a desired number of interference signatures to achieve the best possible classification. The rationale of choosing $\eta=\mathbf{d}^T\mathbf{P}_{\mathbf{U}}\mathbf{d}$ is based on the orthogonal projection correlation between \mathbf{d} and \mathbf{U} . It gives a clue to determining how many additional interference signatures are required for classification and how much orthogonal projection a new signature can contribute. Thus, η can be used as a measure of the information about how many interference signatures need to be generated. If η is small, it implies that most of the significant interference signatures are already contained in the current interference signature set \mathbf{S} . That is, it indicates that the number of generated interference signatures is sufficient to warrant good classification results. Figures 5(a), 5(b), and 5(c) are the rank curves generated by η with the treaded vehicles, the wheeled vehicle, and the object as the designated desired targets, respectively. These are plotted on the basis of the value of η versus the number of interference signatures. Each curve was calculated by using different numbers of VQ-generated interference signatures ranging from 1 to 20. A major disadvantage is computational complexity due to the fact that the VQ-based clustering process must be carried out for each given number of clusters. The classes of interference clusters generated by VQ for different numbers of clusters do not necessarily

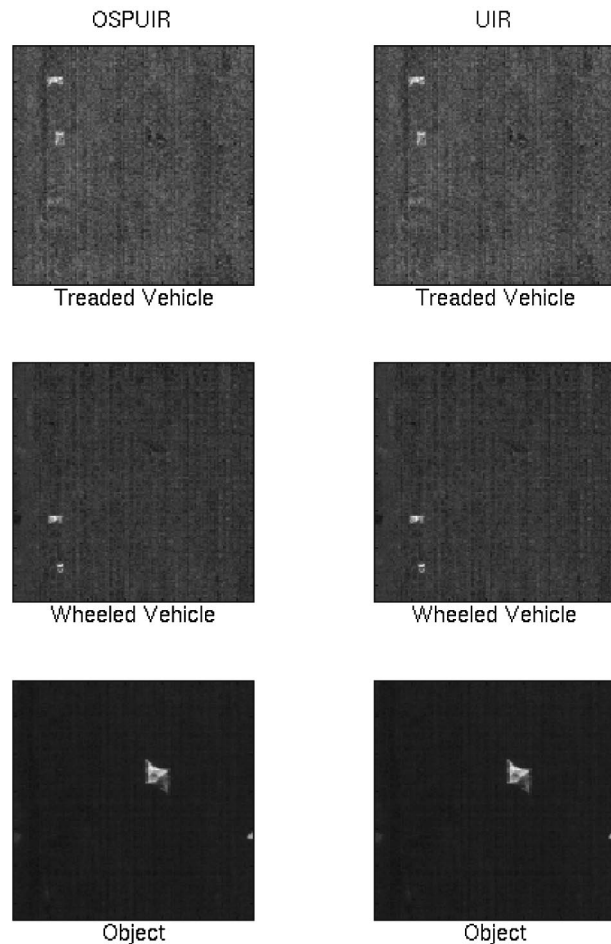


Fig. 4 First column is the results produced by the OSPUIR using $\mathbf{M}=\mathbf{TUBS}$ and the second column is the results produced by the UIR using $\mathbf{M}=\mathbf{TUB}$ and \mathbf{S} as the interference matrix, where \mathbf{S} consists of 10 interference signatures generated by VQ.

embrace one another. For example, the three interference signatures generated by VQ based on $q=3$ are not necessarily included in the class of the five interference signatures based on $q=5$. Some of them may be overlapped, but not necessarily all. This is demonstrated in Fig. 5 where the rank curve is not monotonically decreasing. Figure 6 (where the first column designates treaded vehicles as the desired signature, the second column designates the wheeled vehicle as the desired signature, and the third column designates the object as the desired signature) shows the OSPUIR classification results with 5, 10, 15, and 20 interference signatures. If we choose the number of interference signatures required for classification to be the number at which the rank curve shown in Fig. 5 drops rapidly and sharply, then they are 6 or 10 for the treaded vehicles, 5 for wheeled vehicle, and one of {3,7,11} for the object. Comparing the results in Fig. 6, these numbers may be overestimated a little bit. But they seem still good estimates by considering the fact that no information about interference was given *a priori*. Nevertheless, the number of interference signatures should not be too greatly overestimated. For example, the rank curve of the object classification shown in Fig. 5(c) is completely flat after 11 interference signatures were generated. This is because the η is very

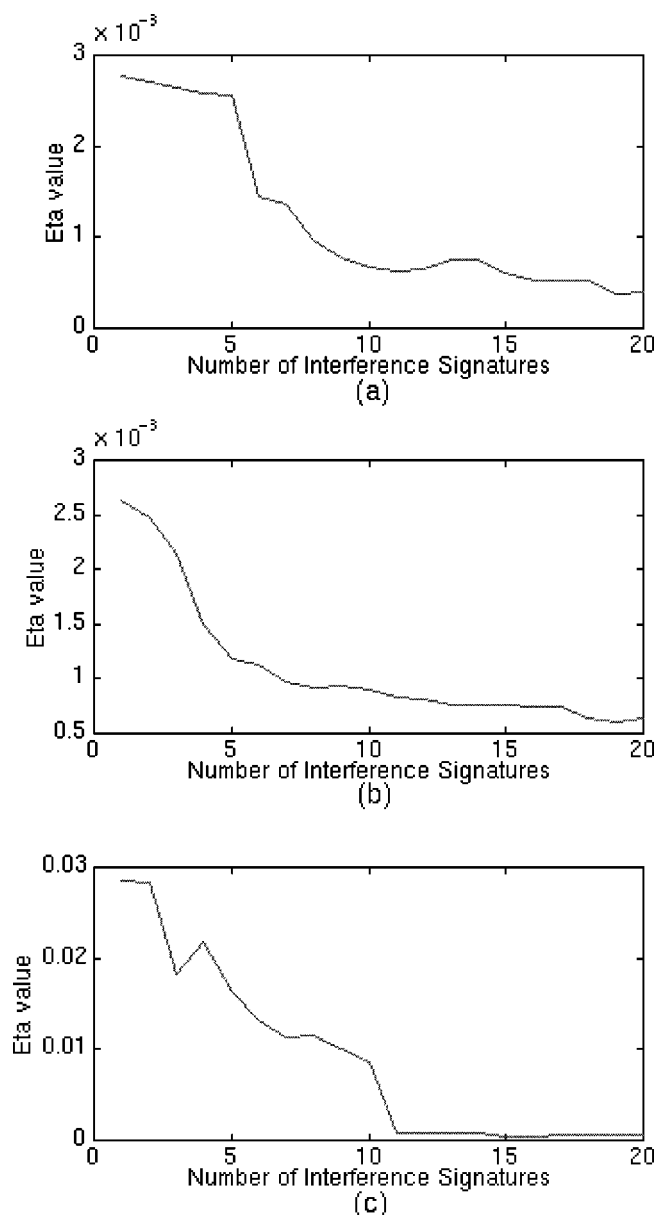


Fig. 5 Rank curves produced by OSPUIR in (a) the treaded vehicle, (b) the wheeled vehicle, and (c) the object classification using from 1 to 20 interference signatures.

small and kept at a constant value, which implies that no improvement can be made by including more interference signatures. While this is true, more interference signatures used for annihilation may even degrade performance as noticed in the third column of Fig. 6 with 20 interference signatures being used. This can be explained as follows. Since the spectrum of the object is very distinct, only a few interference signatures such as natural background are significant and must be nulled prior to classification. These signatures are generally strong interferers and are distinct from the target signatures. If more interference signatures are generated than are needed, we are then forced to find some interference signatures whose spectral characteristics may be similar to that of the target to be classified. As a result, eliminating these signatures may also eliminate part

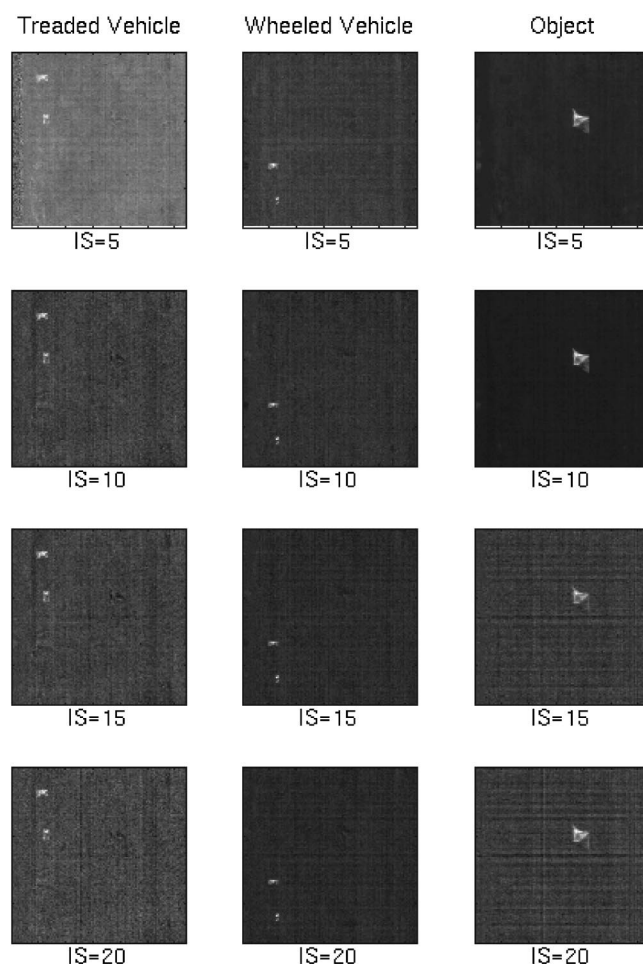


Fig. 6 Images in the first column for the treaded vehicle classification, images in the second column for the wheeled vehicle classification, and images in the third column for the object classification using 5, 10, 15, and 20 interference signatures.

of the spectral characteristics of the target, thus deteriorating the performance. The results justify that the selection of the number of interference signatures as already suggested is indeed a good rule despite the fact that it may be not an optimal one.

Unlike the OSPUIR, which uses η as a criterion for determination of number of interference signatures, the OBSP used the $\text{trace}(E_{\text{MS}}^T E_{\text{MS}})$ as a measure to determine how many interference signatures one needs to generate since the eigenvalues represent the energies of signatures in \mathbf{M} and the $\text{trace}(E_{\text{MS}}^T E_{\text{MS}})$ is the sum of eigenvalues of the interference rejecter E_{MS} . The more interference signatures that are nulled, the less energy is contained in the image, and thus the smaller the $\text{trace}(E_{\text{MS}}^T E_{\text{MS}})$. This does not imply that the rank curve of $\text{trace}(E_{\text{MS}}^T E_{\text{MS}})$ is monotonically decreasing as the number of interference signatures grows due to the same reason given above for $\eta = \mathbf{d}^T \mathbf{P}_0 \mathbf{d}$. Figure 7 shows the rank curve produced by the OBSPUIR using from 1 to 20 interference signatures. It is plotted based on the value of $\text{trace}(E_{\text{MS}}^T E_{\text{MS}})$ versus the number of interference signatures. Note that there is only one rank curve because the $\text{trace}(E_{\text{MS}}^T E_{\text{MS}})$ used for the OBSPUIR depends

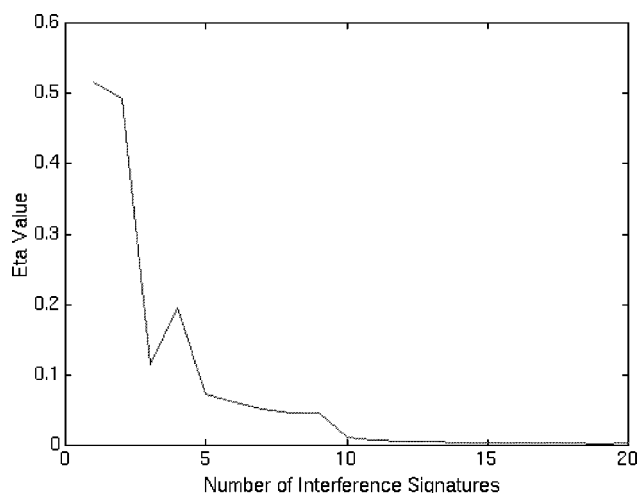


Fig. 7 Rank curve produced by OBSPUIR using from 1 to 20 interference signatures.

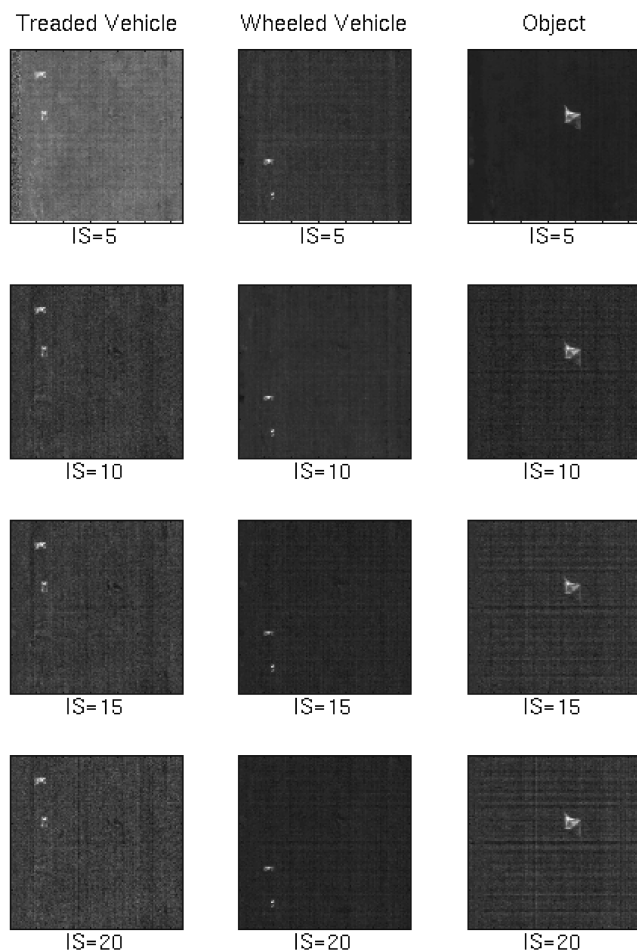


Fig. 8 First, second, and third columns are for the treaded vehicle classification, the wheeled vehicle classification, and the object classification, respectively, with using 5, 10, 15, and 20 interference signatures.

only on the target signature matrix \mathbf{M} and the interference matrix \mathbf{S} , but not the specific targets. The curve drops sharply at 3, increases a little bit at 4, drops again at 5, then gradually decreases until 10, where the curve becomes flat. In this case, we may choose 10 to be the desired number of interference signatures. Figure 8 shows OBSPUIR generated images for each target with 5, 10, 15, and 20 interference signatures. As shown in these images, there is no visible difference between images using more than 10 interference signatures. The results seem to confirm that the proposed eigenvalue criterion successfully predicts an adequate number of interference signatures required for good classification. Since the object has distinctive spectral characteristics different from the treaded and wheeled vehicles, it did not require as many interference signatures as did the vehicles. The same observation made for the object classification using the OSPUIR holds true for the OBSPUIR. This further justifies that the number of interference signatures for target detection and classification depends on the spectral characteristics of the target to be classified.

7 Conclusion

In this paper, a UIR approach was presented to improve the performance of an OSP method,³ which has been successfully applied to AVIRIS and HYDICE data. The idea behind the UIR is to reformulate the commonly used linear spectral mixture model as a linear spectral signature-interference mixture model where the interference is separated from the signature matrix and noise, and treated as a third source. Two UIR-based approaches were presented for this purpose, the OSPUIR and the OBSPUIR. The experimental results show that the OSPUIR and the OBSPUIR significantly improve the OSP-based methods, which use the traditional linear mixture model and discard the interference.

Acknowledgments

The authors would like to thank the Spectral Information Technology Applications Center for providing hyperspectral data set used for experiments in this paper. They also thank the anonymous reviewers for their comments, which greatly improved this paper's quality and presentation.

References

1. G. Vane and A. F. H. Goetz, "Terrestrial imaging spectroscopy," *Remote Sens. Environ.* **24**, 1–29 (1988).
2. A. F. H. Goetz and J. W. Boardman, "Quantitative determination of imaging spectrometer specifications based on spectral mixing models," *IEEE Trans. Geosci. Remote Sens.*, 1036–1039 (1989).
3. J. C. Harsanyi and C.-I. Chang, "Hyperspectral image classification and dimensionality reduction: an orthogonal subspace projection," *IEEE Trans. Geosci. Remote Sens.* **32**, 779–785 (1994).
4. T. M. Tu, C.-H. Chen, and C.-I. Chang, "A posteriori least squares orthogonal subspace projection approach to weak signature extraction and detection," *IEEE Trans. Geosci. Remote Sens.* **35**, 127–139 (1997).
5. C.-I. Chang and C. Brumbley, "An orthogonalization desired signature subspace projection approach to image classification in unknown background," in *Proc. 31st Conf. Information Science and Systems*, pp. 174–178, Johns Hopkins University, Baltimore, MD (1997).
6. X. Zhao, "Subspace projection to multispectral/hyperspectral image classification using linear spectral mixture modeling," MS Thesis, Department of Computer Science and Electrical Engineering, University of Maryland, Baltimore (1996).
7. J. W. Boardman, "Inversion of imaging spectrometry data using singular decomposition," *IEEE Proc. Int. Symposium Geosci. Remote Sens.*, 2069–2072 (1989).
8. R. T. Behrens and L. L. Scharf, "Signal processing applications of

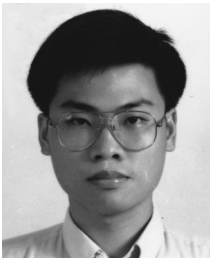
oblique projection operators," *IEEE Trans. Signal Process.* **42**, 1413-1423 (1994).

9. Y. Linde, A. Buzo, and R. M. Gray, "An algorithm for vector quantizer design," *IEEE Trans. Commun.* **28**, 84-95 (1980).
10. I. Katsavounides, C. C. J. Kuo, and Z. Zhang, "A new initialization technique for generalization Lloyd iteration," *IEEE Trans. Signal Process. Lett.* **1**, 144-146 (1994).



Chein-I Chang received his BS, MS, and MA degrees from Soochow University, Taipei, Taiwan, in 1973, the Institute of Mathematics at National Tsing Hua University, Hsinchu, Taiwan, in 1975, and the State University of New York at Stony Brook in 1977, respectively, all in mathematics, and his MS and MSEE degrees from the University of Illinois at Urbana-Champaign in 1982 and his PhD in electrical engineering from the University of

Maryland, College Park, in 1987. He was a visiting assistant professor from January 1987 to August 1987, an assistant professor from 1987 to 1993, and is currently an associate professor in the Department of Computer Science and Electrical Engineering at the University of Maryland, Baltimore County. He was a visiting specialist with the Institute of Information Engineering at the National Cheng Kung University, Tainan, Taiwan, from 1994 to 1995. His research interests include information theory and coding, signal detection and estimation, multispectral/hyperspectral image processing, neural networks, and pattern recognition. Dr. Chang is a senior member of IEEE and a member of SPIE, INNS, Phi Kappa Phi, and Eta Kappa Nu.



Tzu-Lung Sun received his BS degree in computer science from the Chung Cheng Institute of Technology in 1992 and has since been with the An-Kang Computer Center, Taiwan, working on geographic information system (GIS) applications. He is currently on leave and visiting in the Remote Sensing Signal and Image Processing Laboratory within the Department of Computer Science and Electrical Engineering at the University of Maryland, Baltimore County, from 1997 to 1998. His research interests include

remote sensing, image processing, and integrated GIS development.



Mark L. G. Althouse received his BS in physics from the Pennsylvania State University, his MS in electrical engineering from the Johns Hopkins University, and his PhD in electrical engineering from the University of Maryland, Baltimore County (UMBC). Since 1981 he has been with the U.S. Army Chemical and Biological Defense Command at Aberdeen Proving Ground, Maryland working on the remote

detection of chemical vapors and biological aerosols. From 1985 to 1986 he was an exchange scientist at the German NBC Defense Laboratory in Munster. He is currently also a part-time faculty with the Department of Computer Science and Electrical Engineering at the UMBC. His research interests include signal/image processing, signal detection and estimation, pattern recognition, neural networks, and multi- and hyperspectral sensors. Dr. Althouse is a member of SPIE, OSA, IEEE, Tau Beta Pi, and Sigma Xi.